Spt5 C-terminal repeat domain phosphorylation and length negatively regulate heterochromatin through distinct mechanisms

Sarah MacKinnon[1], Viviane Pagé[1], Ryan D. Martin[1], Terence E. Hébert[1], and Jason C. Tanny[1]*

[1]Department of Pharmacology and Therapeutics, McGill University, Montreal, Canada

*corresponding author

Abstract

Heterochromatin is a condensed chromatin structure that represses transcription of repetitive DNA elements and developmental genes, and is required for genome stability. Paradoxically, transcription of heterochromatic sequences is required for establishment of heterochromatin in diverse eukaryotic species. As such, components of the transcriptional machinery can play important roles in establishing heterochromatin. How these factors coordinate with heterochromatin proteins at nascent heterochromatic transcripts remains poorly understood. In the model eukaryote *Schizosaccharomcyes pombe (S. pombe),* heterochromatin nucleation can be coupled to processing of nascent transcripts by the RNA interference (RNAi) pathway, or to other post-transcriptional mechanisms that are RNAi-independent. Here we show that the RNA polymerase II processivity factor Spt5 negatively regulates heterochromatin in *S. pombe* through its C-terminal domain (CTD). The Spt5 CTD is analogous to the CTD of the RNA polymerase II large subunit, and is comprised of multiple repeats of an amino acid motif that is phosphorylated by Cdk9. We provide evidence that genetic ablation of Spt5 CTD phosphorylation results in aberrant RNAi-dependent nucleation of heterochromatin at an ectopic location, as well as inappropriate spread of heterochromatin proximal to centromeres. In contrast, truncation of Spt5 CTD repeat number enhanced RNAi-independent heterochromatin formation and bypassed the requirement for RNAi. We relate these phenotypes to the known Spt5 CTD-binding factor Rtf1. This separation of function argues that Spt5 CTD phosphorylation and CTD length restrict heterochromatin

through unique mechanisms. More broadly, our findings argue that Spt5 CTD repeat length and phosphorylation have distinct regulatory effects on transcription.

Introduction

Transcriptional silencing of repetitive DNA elements proximal to centromeres and telomeres, as well as many developmentally regulated genes, occurs through formation of compacted chromatin structures termed heterochromatin. These structures are propagated through cell division and are thought to underlie epigenetic inheritance (1). Defects in the establishment or propagation of heterochromatin are associated with genome instability and cancer (2–4). Histone modification is central to the formation and propagation of heterochromatin. Methylation of histone H3 on lysine 9 (in pericentric regions) or on lysine 27 (at developmental genes) creates a binding site for chromodomain proteins that mediate chromatin compaction, likely through mechanisms involving liquid-liquid phase separation (5–7).

How heterochromatin is established and maintained at a particular location in the genome is a question that remains unresolved. Evidence from multiple eukaryotic model systems indicates that nascent RNA transcripts produced from heterochromatic loci help to direct heterochromatin formation (8–10). This has been characterized in detail in the model eukaryote *Schizosaccharomyces pombe* (*S. pombe*), in which heterochromatin nucleation is linked to processing of nascent transcripts by the RNA interference (RNAi) pathway (11–13). In *S. pombe*, heterochromatin nucleation sites, often corresponding to

non-coding, inverted repeat sequences within heterochromatin domains, are transcribed by RNA polymerase II (RNAPII) and processed by the double-strand-RNA specific RNase Dicer and RNA-directed RNA polymerase (Rdp1) into siRNAs (14,15). The siRNAs are subsequently bound by the Argonaute family protein Ago1 of the RNA-induced transcriptional silencing complex (RITS) (16–18). siRNA-bound RITS engages heterochromatic nascent transcripts through base-pairing interactions (19). RITS also recruits the histone methyltransferase Clr4, which tri-methylates histone H3 at lysine 9 (H3K9me3) (20). At pericentromeric heterochromatin outer repeats, transcription of the inverted *dg/dh* repeats occurs during S phase, providing a temporal window for RNAi-dependent heterochromatin establishment (21,22). RITS is retained at heterochromatin nucleation sites because its Chp1 subunit is a chromodomain protein that binds to H3K9me3. This creates a self-reinforcing loop that sustains heterochromatin at defined genomic locations (8,13).

H3K9me3 formed through this RNAi-linked pathway is also bound by other chromodomain-containing effector proteins that carry out chromatin condensation, notably the HP1 ortholog Swi6 (23). In addition, Clr4 itself contains a chromodomain that recognizes H3K9me3. This “read-write” mechanism maintains chromatin localization of Clr4, and also leads to methylation of the adjacent nucleosomes and heterochromatin spreading in *cis* (24). The extent to which pericentric heterochromatin spreads is restricted by multiple mechanisms: boundary elements, action of Epe1 (a demethylase-like protein that removes H3K9me3), and action of other euchromatic chromatin-modifying factors that promote histone turnover (25–28). The siRNAs produced from

heterochromatic loci are also prevented from spreading in *trans*, i.e. targeting a homologous sequence distant from their site of origin (29,30). Restriction of *trans*-silencing seems to involve regulation of transcription elongation and proper mRNA 3' end processing, as mutants that disrupt these processes have been found to allow siRNA-directed heterochromatin formation at ectopic locations (29). ~20 such mutations have been identified, including mutations in members of the Polymerase Associated Factor (PAF) complex and Prf1/Rtf1 (29,31,32). This highlights the fact that the RNAi machinery must act within the context of the general RNA polymerase II (RNAPII) transcriptional apparatus to establish heterochromatin.

Although the RNAi-dependent pathway is required for *S. pombe* pericentromeric heterochromatin formation, parallel mechanisms that are independent of RNAi also contribute, and may play more important roles at other heterochromatic loci. These include post-transcriptional silencing mechanisms involving transcription termination factors, the nuclear exosome complex, and mRNA elimination factors. Transcriptional silencing mechanisms involving stress-responsive transcription factors or a histone deacetylase complex have also been implicated (33–39). Interestingly, contribution of RNAi-independent mechanisms to pericentric heterochromatin can be revealed in RNAi mutants, which can be suppressed by inactivation of several factors regulating RNAPII elongation or mRNA processing (40,41). This further underscores the complex interplay between transcription and heterochromatin formation.

The *S. pombe* model system has been powerful in revealing mechanisms of co-transcriptional assembly of heterochromatin. However, many key questions remain, including how the general transcription machinery interfaces with heterochromatin proteins and what prevents these interactions at transcribed genes. We investigated these questions through study of Spt5, a conserved, essential RNAPII elongation factor. Eukaryotic Spt5 is required for processive RNAPII elongation, and also promotes RNAPII stability and enhancer function (42–45). Cryo-electron microscopy structures of Spt5 in complex with elongating RNAPII show that Spt5 maintains the RNAPII transcription bubble by forming “clamps” around the DNA template and the exiting RNA. The clamps are formed by NGN (NusG N-terminal) and KOW (Kyprides, Ouzounis, Woese) domains that are conserved in prokaryotic, eukaryotic, and archaeal Spt5 orthologs (46,47). Eukaryotic Spt5 orthologs also contain a C-terminal domain (CTD; also called a C-terminal region or CTR) that is comprised of multiple repeats of a 6-9 amino acid motif (48,49). Like the analogous CTD on the RNAPII large subunit, the Spt5 CTD interacts with factors involved in elongation, mRNA processing, and histone modification. Whereas the Rpb1 CTD is phosphorylated by multiple kinases, the Spt5 CTD is primarily targeted by Cdk9 (50). Cdk9-dependent phosphorylation of the Spt5 CTD enhances RNAPII elongation rate and processivity, and promotes co-transcriptional histone modifications (44,51–54). These effects are mediated at least in part by Rtf1 (Prf1 in *S. pombe*), the only known phospho-specific CTD interactor (55,56). Rtf1 directly stimulates the ubiquitin-conjugating activity of Rad6, leading to histone H2B monoubiquitylation (H2Bub1) and subsequent H3 lysine 4 methylation (H3K4me) (57). It also stimulates elongation rate by binding directly to RNAPII (58,59). The unphosphorylated CTD binds to mRNA capping

and 3'-end processing factors (60–62). The Spt5 CTD is generally more variable in repeat sequence and number between species than the RNAPII CTD. *S. pombe* Spt5 harbors an unusually regular and uniform CTD comprised of 18 repeats of a nonapeptide motif (TPAWNSGSK) that is phosphorylated by Cdk9 on Thr1 (63,64).

Since Prf1/Rtf1 was identified as a factor that restricts *trans*-silencing, we hypothesized that the Spt5 CTD also acts to limit co-transcriptional heterochromatin formation. We tested Spt5 CTD mutants that differed in repeat length and sequence for effects on heterochromatin formation. Interestingly, we found evidence that repeat length and phosphorylation state of the Spt5 CTD distinctly regulate RNAi-dependent and RNAi-independent heterochromatin pathways.

Results

Spt5 CTD phosphorylation blocks trans-silencing by heterochromatin-derived siRNAs

To determine if the Spt5 CTD has a shared function with the PAF complex and Prf1/Rtf1 in negatively regulating siRNA-mediated *de novo* heterochromatin formation, we used a dual *ade6*$^+$ reporter system in which the *ade6*$^+$ marker is present at its endogenous, euchromatic location and at a second location within pericentric heterochromatin (32). The heterochromatic *ade6*$^+$ acts as a source of *ade6*+-derived siRNAs (Fig. 1A). In wild-type cells, these siRNAs can only act on the heterochromatic *ade6*$^+$, such that the euchromatic copy is fully expressed and all the cells form white colonies on adenine-

limiting media. Mutations affecting PAF components (or other regulators of transcription elongation and mRNA export) allow the siRNAs produced from the heterochromatic *ade6*$^{+}$ to act in *trans*, resulting in *de novo* heterochromatin formation at the endogenous *ade6*$^{+}$ locus in a fraction of the mutant cells. These events are scored as red colonies on adenine-limiting media (32).

We introduced this reporter system into two sets of *spt5* mutant strains: one that harbored substitutions in T1 of the nonapeptide CTD motif in each of the 18 repeats in the full-length protein [*spt5(18)*], and one that harbored the same substitutions in the context of a truncated, 7-repeat CTD [*spt5(7)*] (65). This allowed independent assessment of the effects of repeat length and T1 phosphorylation state in the assay. We also included a strain in which the entire CTD was deleted (*spt5ΔC*) (65). The *spt5(7)-T1A, spt5(18)-T1A,* and *spt5ΔC* strains exhibited ~4-8% red colonies when plated at single-cell density, a frequency similar to that observed for highly penetrant drivers of siRNA-mediated *trans*-silencing in this and similar reporter systems (31,32). (Fig. 1B and 1C). Wild-type controls and *spt5-T1E* strains showed zero penetrance of the red phenotype. Thus, Spt5 T1 phosphorylation, or installation of a constitutive negative charge at this position, blocks siRNA-mediated silencing in trans.

To confirm that the observed *trans*-silencing correlated with *de novo* heterochromatin formation, we first assessed the mitotic stability of the red colony phenotype in re-plating assays. As observed for other mutants that enhance trans-silencing, red colonies gave rise to a mixture of red and white colonies upon re-plating to adenine-limiting media, with red predominating over white. This is consistent with the red colony phenotype arising due to *de novo* heterochromatin formation (Fig S1A). We next

performed anti-H3K9me3 ChIP-qPCR using cells derived from red and white *spt5-T1A* and *spt5ΔC* colonies. A *clr4*Δ strain, in which H3K9 methylation is absent, was included as a control for antibody specificity. H3K9me3 enrichment at *vtc4*$^{+}$*,* a gene adjacent to the endogenous copy of *ade6*$^{+}$*,* was increased between 4-fold and 12-fold in red colonies compared to white colonies for *spt5(7)-T1A, spt5(18)-T1A,* and *spt5ΔC* (Fig. 1D) (32). These changes were statistically significant in the *spt5(7)-T1A* and *spt5ΔC* strains. H3K9me3 enrichment at *vtc4*$^{+}$ in the red *spt5(18)-T1A* isolates was more variable but still suggestive of ectopic heterochromatin formation. Overall, these results indicated that pSpt5, independent of Spt5 CTD repeat number, is involved in repressing ectopic siRNA-mediated heterochromatin formation.

Spt5 CTD phosphorylation prevents expansion of pericentric heterochromatin in *cis*

We next considered whether Spt5 CTD phosphorylation is important for regulating heterochromatin domains at their normal chromosomal locations. To this end, we utilized a *ura4*$^{+}$-based reporter assay to detect heterochromatin spreading outside a boundary element flanking pericentric heterochromatin on chromosome I (*irc1*). The *irc1L::ura4*$^{+}$ reporter lies just outside this boundary and is fully expressed in wild-type cells, conferring sensitivity to the counterselection drug 5-fluoroorotic acid (5'FOA)(Fig. 2A) (66). *spt5-T1A* and *spt5ΔC* strains harboring this reporter showed enhanced growth compared to control in the presence of 5'FOA, suggesting that the reporter is silenced in some fraction of the mutant cells (Fig. 2B and 2C). This was dependent on the positioning of *ura4*$^{+}$ outside *irc1L,* as all Spt5 CTD variant strains expressing *ura4*$^{+}$ from its endogenous locus grew

similarly to controls (Fig. S2A). These results argue that *spt5-T1A* and *spt5ΔC* variants that allow siRNA-mediated ectopic heterochromatin nucleation also result in increased heterochromatin spreading at *irc1*. We performed ChIP-qPCR on *spt5-T1A*, *spt5-T1E, spt5ΔC,* and control strains grown under non-selective conditions, but were unable to detect increases in H3K9me2 or H3K9me3 proximal to *irc1* that correlated with the results of the 5'FOA spot tests (Fig S2A-C). This is likely because increased heterochromatin spreading is a rare event affecting a small percentage of cells in the mutant strains. The fact that we were unable to detect a decrease in growth on -ura media in the mutant strains harboring the *irc1L::ura4*$^{+}$ reporter is also consistent with the Ura- phenotype arising in a small fraction of the cells (Fig 2B).

Truncation of the Spt5 CTD renders pericentric heterochromatin RNAi-independent

Our results pointed to a negative regulatory role for Spt5 CTD phosphorylation in RNAi-dependent heterochromatin formation. To test whether the Spt5 CTD may also negatively regulate RNAi-independent heterochromatin formation, we generated double mutants combining each of the Spt5 CTD variants with *ago1Δ.* The *ago1*$^{+}$ gene encodes the sole Argonaute family protein in *S. pombe*, which mediates siRNA action on heterochromatin. Pericentric heterochromatin is strongly dependent on *ago1*$^{+}$, but some residual, RNAi-independent heterochromatin is present in *ago1Δ* and can be enhanced in some elongation/mRNA export mutants (40,67). We utilized the microtubule-destabilizing agent thiabendazole (TBZ) as a proxy for pericentric heterochromatin integrity; mutants deficient in pericentric heterochromatin impair centromere function and spindle-kinetochore attachment, resulting in sensitivity to TBZ. Strikingly, truncating the

Spt5 CTD to 7 repeats rescued the TBZ-sensitivity of *ago1Δ* (Fig. 3A). This phenotype was independent of Spt5 CTD T1 phosphorylation, as it was caused by *spt5(7), spt5(7)-T1A,* and *spt5(7)-T1E* mutations (albeit more weakly in the T1 mutants). Moreover, complete removal of the Spt5 CTD by the *spt5ΔC* mutation was *not* able to rescue *ago1Δ* in this assay and displayed TBZ sensitivity on its own. This suggests that this mutation impacts additional mechanisms related to centromere function. An identical pattern of suppression was obtained when these Spt5 CTD mutations were combined with a knockout of the *S. pombe* Dicer ortholog, *dcr1Δ* (Fig. S3A). These results suggested that reduction of Spt5 CTD repeat number may bypass the requirement for the RNAi pathway in formation of pericentric heterochromatin.

To further test this idea, we performed anti-H3K9me3 ChIP-qPCR with primers that amplify the *dh* repeat region within pericentric heterochromatin. Deletion of *ago1*$^{+}$ in an otherwise wild-type background reduced H3K9me3 enrichment by ~6-fold. The reduction caused by *ago1Δ* was not significant in *spt5(7)* and *spt5(7)-T1E* double mutants, was ~3.5-fold in the *spt5(7)-T1A* double mutant, and was >10-fold in the *spt5ΔC* double mutant (Fig. 3B). Thus, the requirement for *ago1*$^{+}$ for pericentric H3K9me3 was bypassed by the *spt5(7)* and *spt5(7)-T1E* alleles, but not *spt5(7)-T1A* or *spt5ΔC.* Bypass by *spt5(7)* was also apparent when H3K9me3 enrichment was assessed using a primer pair located near the *irc1R* heterochromatin domain boundary (Figure S3B). At this location, both T1 mutant *spt5(7)* variants failed to bypass *ago1Δ,* indicating that the suppressive effect of reduced Spt5 CTD repeat number could be modulated by mutations of T1.

We also measured the levels of heterochromatic transcripts in these strains using strand-specific RT-qPCR. Consistent with previous results, *ago1Δ* increased the levels of

forward-strand transcripts and led to a smaller increase in transcripts corresponding to the reverse strand (Figure 3C)(11). These effects were abrogated in the *spt5(7) ago1Δ* double mutant. However, the *spt5(7)* T1 variants (and *spt5ΔC)* failed to suppress *ago1Δ* in this assay, arguing that suppression by a short Spt5 CTD requires the T1 residue.

To further probe the relationship between Spt5 CTD phosphorylation and repeat number, we constructed double mutants of full length Spt5 CTD T1 point mutants with *ago1Δ* [*ago1Δ spt5(18)-T1A* and *ago1Δ spt5(18)-T1E)*]. Growth of these strains on TBZ media showed that blocking or mimicking phosphorylation at this site did not rescue the sensitivity of *ago1Δ* (Fig. 4A). Correspondingly, H3K9me3 ChIP-qPCR enrichment levels are significantly decreased in each double mutant at both the *dh* element and outside *irc1R* when compared with each corresponding full length Spt5 CTD point mutant (Fig. 4B and S3C). Thus, Spt5 CTD T1 phosphorylation restricts the RNAi-dependent heterochromatin pathway and heterochromatin spreading, whereas Spt5 CTD repeat number restricts RNAi-independent heterochromatin formation in a manner that depends on Spt5 CTD T1 (Figure 4C).

Evidence that Prf1/Rtf1 is an effector for the Spt5 CTD in regulating heterochromatin

Given that Spt5 CTD T1 phosphorylation creates a binding site for the Plus3 domain of Prf1/Rtf1, we queried *prf1* mutants for similar effects on heterochromatin regulation. Wild-type or mutant versions of Prf1 fused to a TAP-tag were expressed in the dual *ade6*$^{+}$ reporter strain (68); the wild-type *prf1-TAP* did not give rise to any red colonies (Fig 5A). Point mutations in the Plus3 domain that impair Prf1 association with chromatin

activated trans-silencing of euchromatic *ade6*$^{+}$. This was true for *prf1-R227A*, known to abrogate phospho-specific binding to the Spt5 CTD, as well as *prf1-R262E* and *prf1-R296E*, which affect an as-yet unknown Plus3 domain interaction (68). C-terminal truncation of Prf1 (*prf1ΔC1-345*) also allowed *trans*-silencing in this strain. This form of Prf1 is recruited to chromatin normally but lacks protein segments that bind to PAF complex components and to RNAPII (59,68,69). A shorter C-terminal truncation of *prf1*$^{+}$ was previously shown to have the same effect (29). These data are consistent with the notion that Spt5 T1 phosphorylation negatively regulates *de novo*, siRNA-dependent heterochromatin formation by promoting recruitment of functional Prf1/Rtf1 to chromatin.

The heterochromatin spreading phenotypes displayed by *spt5-T1A* and *spt5ΔC* were also shared by *prf1*$^{+}$ variants that activated *trans*-silencing of euchromatic *ade6*$^{+}$ (Fig. 5B). The *prf1-R227A, prf1-R262E,* and *prf1ΔC1-345* mutations exhibited increased growth in the presence of 5'FOA in strains harboring the *irc1L::ura4*$^{+}$ reporter construct. The *prf1-R296E* mutation, which had a weak phenotype in the dual *ade6*$^{+}$ reporter strain (and causes only partial loss of Prf1 chromatin binding), did not lead to heterochromatin spreading beyond *irc1L.* These data further support a negative role for Prf1/Rtf1 in heterochromatin regulation.

Surprisingly, *prf1-R227A* and *prf1-R262E* mutations also suppressed the TBZ sensitivity of *ago1Δ* compared to the wild-type *prf1-TAP* control (Fig 5C). This suggests a strengthening of RNAi-independent silencing mechanisms in these mutants, in addition to the effects on RNAi-dependent mechanisms described above. While *prf1-R227A*

mirrors *spt5(18)-T1A* in its effects on *trans*-silencing, the same is not true with respect to their effects on RNAi-dependent heterochromatin regulation. This is consistent with our previous observations that pSpt5 and the Plus3 domain of Prf1/Rtf1 have functions beyond the Cdk9-Spt5-Rtf1 pathway; our evidence suggests this also extends to regulation of heterochromatin (68).

Discussion

Our results demonstrate that the Spt5 CTD negatively regulates heterochromatin in *S. pombe*. We observed a clear functional separation between different Spt5 alleles with respect to effects on heterochromatin: substitution of Spt5 T1 in the CTD repeats led to enhancement of heterochromatic silencing through the RNAi pathway, whereas reduction in Spt5 CTD repeat number led to increased RNAi-independent silencing. These findings argue that silencing factors in the RNAi-dependent pathway engage the transcriptional machinery differently from those in the RNAi-independent pathway, and that the biological effects of Spt5 CTD length and phosphorylation can be separated. Finally, a mutation in the CTD-interacting factor Prf1/Rtf1 exhibited a similar separation of function, suggesting that it is involved in mediating the effects of the CTD on heterochromatin.

To our knowledge, this is the first study to identify separation of function alleles in the same gene that differentially regulate RNAi-dependent and RNAi-independent heterochromatic silencing. Comparison of this unique phenotypic profile to that of other negative regulators of heterochromatin is informative regarding the potential mechanisms

involved. Mutations in subunits of the Cleavage and Polyadenylation Factor (CPF) complex, a major mRNA 3'-end processing factor, cause phenotypes similar to those we observed for *spt5-T1A*, as they allow small RNA-dependent trans-silencing but do not enhance (and in some cases impair) RNAi-independent silencing (31,34,38). These include knockouts of genes encoding the phosphatase module subunits of CPF (*dis2*$^{+}$*, ppn1*$^{+}$*, swd2.2*$^{+}$*, ssu72*$^{+}$) and loss-of-function alleles in genes encoding cleavage module subunits (*yth1*$^{+}$*, pfs2*$^{+}$*, ctf1*$^{+}$). The CPF mutant phenotypes suggest that slowing of transcript cleavage and release may enable *trans*-silencing by shifting kinetic competition between mRNA 3'-end processing and the RNAi pathway toward the latter (29,31). The *spt5-T1A* phenotype is not likely due to a decrement in transcript cleavage, since *spt5-T1A* reduces RNAPII processivity and leads to *enhanced* termination (70). Moreover, removal of Dis2, the Spt5 T1 phosphatase, would be expected to phenocopy a *spt5-T1E* mutant, not *spt5-T1A*. Slow elongation caused by *spt5-T1A* (likely by impairment of Prf1/Rtf1 function) may favor association of the RITS complex with nascent transcripts. Alternatively, *spt5-T1A* may perturb association of other factors with nascent transcripts. This could explain the phenotypes of *trans*-silencing enabling mutants such as those affecting the PAF complex, or the mRNA export factors Mlo3 and Dss1 (29,32). The cryo-EM-derived structure of a RNAPII elongation complex supports this notion: the Spt5 CTR (bound by the Rtf1 Plus3 domain) and the C-terminal extension of the PAF subunit Leo1 are positioned in close proximity to the RNA exit channel and the exiting RNA on the upstream side of the elongating polymerase (59). However, *leo1Δ* and *mlo3Δ* enhance both RNAi-dependent and RNAi-independent silencing pathways, indicating that *spt5-*

T1A must cause a more subtle or specific structural alteration to the elongation complex (40,71).

The spreading of heterochromatin beyond the *irc1L* boundary in the *spt5-T1A* mutant is consistent with the positive role of pSpt5 in regulating chromatin-modifying factors. pSpt5 directly recruits Prf1/Rtf1 to chromatin, which in turn stabilizes PAF complex chromatin association (56). It is thus a key intermediate in the pathway linking Cdk9 activity to co-transcriptional histone modifications H2Bub1 and H3K4me. Stimulation of histone turnover by the PAF complex and by the Set1 H3K4 methyltransferase complex has been shown to counteract aberrant heterochromatin spreading (26,71).

Truncation of the Spt5 CTD specifically enhanced RNAi-independent silencing. Altered interactions with the nascent transcript could likewise explain this effect, given that RNAi-independent silencing has been linked to premature RNAPII termination. Premature termination is promoted by a suite of termination factors, including the CPF complex, and is opposed by TFIIS, a factor that prevents elongation stalling due to polymerase backtracking (33,34,38,67). How Spt5 CTD truncation participates in this mechanism remains to be determined. The fact that T1 mutations in the context of the short CTD partially prevented bypass of *ago1Δ* for heterochromatin formation suggests that the T1 residue has a dual function: it blocks aberrant spread of heterochromatin linked to RNAi, both in *cis* and in *trans*; and it *promotes* RNAi-independent heterochromatin formation. Furthermore, the two functions may involve distinct interactions: the former is supported by phenotypes exhibited by *spt5-T1A* and not *spt5-T1E*, whereas the latter is supported by a phenotype exhibited by both variants.

Enhanced *trans*-silencing and heterochromatin spreading seen in the *spt5ΔC* variant are consistent with a negative regulatory role for pSpt5: lack of pSpt5 in the absence of the Spt5 CTD likely underlies why *spt5ΔC* and *spt5-T1A* behaved similarly in these assays. We expected that *spt5ΔC* may share phenotypes with the truncated, 7-repeat version of *spt5* as well. However, complete CTD removal did not suppress the heterochromatin defect in *ago1Δ*, despite the fact that CTD truncation did. Germane to this difference is the fact that *spt5ΔC* was slightly TBZ-sensitive on its own, suggesting that CTD truncation beyond a minimum repeat length reveals an additional role in centromere function that masks the inhibitory effect of the CTD on RNAi-independent heterochromatin. In addition, the suppression of *ago1Δ* also required the T1 residue of the CTD repeat, which is absent in *spt5ΔC*.

We identified an allele of *prf1*+, *prf1-Δ345*, that exhibited a similar separation of function as the *spt5-T1A* mutation: RNAi-dependent heterochromatin was enhanced, spreading in *cis* was enhanced, but RNAi-independent heterochromatin was not. This suggests that Prf1/Rtf1 likely acts downstream of Spt5 T1 phosphorylation, consistent with the fact that it specifically binds to pSpt5. The C-terminal portion of Prf1 removed by *prf1-Δ345* has been shown, in biochemical assays, to directly contact the PAF complex and RNAPII, and to stimulate RNAPII elongation rate (59). Surprisingly, point mutations within the Plus3 domain of Prf1, the domain that binds to pSpt5 and is required for Prf1 recruitment to chromatin, do not show similar phenotypic specificity as they impacted both RNAi-dependent and RNAi-independent pathways. Moreover, the variant of Prf1 encoded by *prf1-Δ345* associates with chromatin normally, arguing that it impairs Prf1 function differently than loss of pSpt5 (68). These findings reinforce our previous

observation that the Plus3 domain function does not simply equate with Prf1 recruitment, and is distinct from that of pSpt5. We speculate that *prf1-Δ345* compromises an interaction between chromatin-bound Prf1 and another factor. This would be similarly affected by Plus3 domain mutations that decrease the stability of Prf1 chromatin association; however, our data suggest that these mutations must also affect another Prf1 function.

Whereas Spt5 CTD phosphorylation is known to regulate specific CTD interactions, the impact of repeat number on Spt5 CTD function has not been examined in detail, and likely has important general implications for CTD function in transcription. Based on the properties of the Rpb1 CTD, it is intriguing to speculate that the effects of repeat length are attributable to changes in the formation of transcription foci that form by liquid-liquid phase separation (72). For the Rpb1 CTD, the number of repeats required to sustain function *in vivo* correlates with the biophysical property of phase separation *in vitro.* Phosphorylation of the repeats alters phase separation behavior, and can have a positive or negative effect on foci formation (73). Formation of phase separated transcription foci has been primarily implicated in early stages of transcription, and there is little known about how these kinds of structures might regulate post-initiation steps. However, there is evidence that a phase separation mechanism is involved in co-transcriptional histone H2B monoubiquitylation (74). Further exploring this question, and a potential role for the Spt5 CTD and Rtf1/Prf1, are important future avenues of investigation.

Materials and Methods

Yeast strains and media. Yeast strains used in this study are listed in Table 1. To generate the *spt5(18)-T1A* and *spt5(18)-T1E* strains, in which T1 is replaced by alanine or glutamate in every repeat of the full-length spt5-CTD (JT1047, JT1048, JT1049), integration cassettes were constructed by replacing a *spt5*$^{+}$ gene fragment (+2398 of the *spt5* ORF to the stop codon) in the pUC19-based spt5^{CTD+}-ura4-spt5$^{3'}$ plasmid (75) with synthetic DNA fragments (Genscript) harboring the relevant mutations. The spt5$^{T1A/T1E}$ – ura4^{+}–spt5$^{3'}$ cassettes were excised and transformed into *S. pombe* using standard methods (77). Ura+ transformants were selected and analyzed by diagnostic Southern blotting and sequencing of PCR-amplified DNA segments to verify correct integrations.

Strains harboring *ade6*$^{+}$ reporter genes were constructed by mating and tetrad dissection using standard methods (76). Presence *of ade6*+ within *otr1* in adenine prototroph isolates was confirmed by PCR with primers indicated in Table 2 (Dg'Fw and Ade6'Rv).

The *spt5(7)-WT, spt5(7)-T1A,* and *spt5(7)-T1E* alleles were introduced into an *IRC1L*::*ura4*$^{+}$ reporter strain in two steps. First, *per1::natMX6* was switched to *per1::hphMX6* in strain JT793 (Table 1) by transformation with a *hphMX6* PCR product amplified from plasmid pFA6-hphMX6 (77) to generate strain JT1030. Next, *natMX6*-marked *spt5(7)-WT, spt5(7)-T1A,* and *spt5(7)-T1E* alleles were excised from pUC19-based spt5^{CTD+}-nat-spt5$^{3'}$ plasmids (versions of the spt5^{CTD+}-ura4-spt5$^{3'}$ plasmids described above which contained a truncated CTD array and a *natMX6* cassette instead of *ura4*$^{+}$; a gift from B. Schwer) and transformed into strain JT1030. Correct integration was verified by diagnostic PCR and sequencing. The *natMX6*-marked versions of

spt5(18)-T1A and *spt5(18)-T1E* alleles were generated by transformation of strains JT1047, JT1048, and JT1049 (Table 1) with a *natMX6* cassette (amplified from pFA6-natMX6 (77) with primers Spt5Ura4'Fw and Spt5Ura4'Rv). These strains (JT1192, JT1193, and JT1194) were crossed to JT1030 to introduce the *IRC1L*::*ura4*$^+$ reporter gene.

Double mutants with *ago1*Δ were constructed by mating and random spore disruption as described previously; haploid double mutant isolates were verified by mating tests and PCR (78).

YES and pombe minimal glutamate (PMG) media were as described previously (77). Thiabendazole (TBZ; Sigma) was used at a concentration of 15 □g/L. 5'-fluoroorotic acid (5'FOA; Sigma) was used at a concentration of 1 g/L in PMG containing 45 mg/L uracil. Spot dilution tests were carried out as described previously (68). Plates were incubated at 30 degrees for 3 to 7 days before imaging.

Chromatin immunoprecipitation. Chromatin from 1.5x10^7 *S. pombe* cells was prepared as described previously (79). For H3K9me3 ChIP, 50 μL of spike-in chromatin (*S. cerevisiae* BY4743 expressing *TFB1-myc*) was mixed with each 1 mL sample prior to taking a 100 μL input sample. The lysate was precleared by incubating with 15 μL dynabeads M-280 straptavidin (Invitrogen by ThermoFisher), pre-equilibrated with 1 mL lysis buffer [50 mM Hepes pH 7.5, 150 mM NaCl, 1 mM EDTA, 1 % Triton X-100, 0.1 % Na deoxycholate, 1 mM PMSF, protease inhibitor tablet (Roche) (one mini tablet per 10 mL)] for 2 hours. For each sample, 20 μL of dynabeads were washed with 100 μL 0.5% BSA in TBS (TBS/BSA) twice. 0.5 μg (2 ul) of H3K9me3 antibody (Diagenode) and 0.5

μL of biotin-myc antibody (Abcam) were diluted into 0.5% BSA in TBS to a total volume of 200 μL, and incubated with beads for 1 hour at 4 degrees. The beads were washed with TBS/BSA containing 5 μM biotin for 10 minutes at 4 degrees twice. The beads were washed twice with 500 μL lysis buffer, and transferred into a new low-protein binding tube. The cleared lysate was incubated with the antibody-bound beads overnight, then beads were washed and eluted as described previously. In the final step of the IP clean up, beads were washed with TE instead of TE + SDS 0.75% in order to reduce the concentration of SDS to 0.4%.

For H3K9me3 ChIP of red and white colonies from *ade6*$^{+}$ reporter strains, a single red or white colony that arose from each strain after growth on PMG low adenine (7 mg/L adenine) plates was grown in 2 mL of PMG low adenine (30 mg/L adenine) overnight. Small cultures were used to inoculate 50 mL cultures in PMG low adenine (30 mg/L adenine) and grown overnight prior to formaldehyde crosslinking and ChIP. No spike-in chromatin was used.

For H3K9me2 ChIP, chromatin was extracted from *S. pombe* cells as described previously (79). 13 μg of spike-in chromatin (prepared from NIH 3T3 cells) was mixed with each 1 mL sample prior to taking a 100 μL input sample. 3 μg of H3K9me2 antibody (Abcam) was added to the remaining ~900 μL of lysate and the remaining IP steps were carried out as described previously using 20 μL Dynabeads protein G (Invitrogen by ThermoFisher) per sample. In the final step of the IP clean up, beads were washed with TE instead of TE + SDS 0.75% in order to reduce the concentration of SDS to 0.4%.

To reverse crosslinking of ChIP samples, the ~250 μL samples were incubated in a dry bath at 65 degrees overnight. ChIP input samples were diluted with 150 μL TE to a total volume of 250 ul, to reduce SDS concentration to 0.4% before reversing crosslinking at 65 degrees overnight.

Purification of DNA from ChIP samples was as described (79) with the following modifications. Samples were not further diluted with TE following crosslinking, phase extraction steps were carried out using a volume of 250 μL phenol:chloroform:isoamyl alcohol 25:24:1, and then again using the same volume of chloroform. Following phase extraction steps, 3 M sodium acetate (pH 5.3) was added to the aqueous phase to a concentration of 300 μM, and 2 μL glycogen was added to facilitate DNA precipitation. Samples were incubated at -20 degrees for at least 12 hours, then centrifuged at 14000g for 30 min. The DNA was recovered, washed with 1 mL 70% ethanol, dried and resuspended in 50 μL TE.

Spike-in chromatin preparation. Chromatin from *S. cerevisiae* strain BY4743 expressing *TFB1-myc* was used as a spike-in for H3K9me3 ChIP. The anti-myc antibody (Abcam ab81658) was used to IP *TFB1-myc* and qPCR was performed with primers amplifying the promoter of *S cerevisiae* gene *PMA1.* 3.0×10^7 *S. cerevisiae* cells were used for chromatin extraction as described previously; 50 μL of *S. cerevisiae* chromatin was added per 1 mL of *S. pombe* chromatin to give a cell:cell ratio of 1:20 (79).

Chromatin from NIH 3T3 cells was used as a spike-in for H3K9me2 ChIP. No additional spike-in antibody was added; the anti-H3K9me2 antibody (Abcam) was used to IP H3K9me2 and detected by qPCR with primers amplifying the promoter of the *M. musculus* gene *Pou5f.* NIH 3T3 cells were grown to confluency in 18 mL DMEM + ITS + P/S in 15 cm plates. Media was replaced with 18 mL 1% formaldehyde in DMEM, and cell cultures were agitated slowly on a shaker for 15 min. 2 mL 1.25 M glycine was added to a concentration of 0.125 mM; plates were agitated slowly for 5 min to quench the crosslinking reaction. Plates were transferred to ice then washed with cold PBS. Cells were transferred by adding 4 mL PBS + 1mM PMSF and centrifuged for 5 min at 800g. The cell pellet was resuspended in 1 mL cell lysis buffer (10mM Tris-HCl pH 8.0, 10mM EDTA, 0.5 mM EGTA, 0.25% Triton X-100 with 1mM PMSF and 5 μL PIC (protease inhibitor cocktail, Sigma P8340) and incubated at 4 degrees for 10 min. Cells were centrifuged at 800g for 5 min to remove cell lysis buffer and resuspended in 100 μL nuclei lysis buffer, (50mM Tris-HCl pH 8.0, 10 mM EDTA, 1% SDS with 1mM PMSF 5 μL PIC/1mL buffer) then incubated on ice for 15 min. The lysate was sonicated (Bioruptor water-bath sonicator) to shear the chromatin for 15 min, 30 seconds on/off on the high setting. The chromatin was cleared by centrifugation at 14000g for 15 min, then stored at -80 degrees prior to IP. A 10 μL sample was taken for DNA clean up and quantification prior to storage.

RT-qPCR. Isolation of RNA and strand-specific RT-qPCR were performed as described previously, with 1 μg RNA per strain for *act1*$^{+}$ RT and 5 μg RNA for *dh*. (79). Transcript levels obtained with *dh* repeat primers were normalized to *act1*$^{+}$.

***Trans*-silencing assays.** Control and mutant strains containing the *ade6*+ reporter construct were grown in 2 mL YES cultures. Once the cultures reached early log phase (OD_{600} ~0.100-0.300) the cell concentration was determined with a haemocytomer. ~1000 cells per condition were plated on a single PMG low adenine plate (pombe minimal glutamate media with 7 mg/L adenine), and incubated at 30 degrees for 7 days. The plates were stored at 4 degrees for 24 hours prior to imaging. ImageJ software was used to quantify the number of red and white colonies on each plate.

Acknowledgements

We thank B. Schwer, R. Fisher, E. Bayne, and D. Moazed for providing *S. pombe* strains, and B. Schwer for providing plasmids. We thank B. Schwer, S. Shuman, and members of the Tanny lab for helpful discussions. This work was funded by the Canadian Institutes of Health Research (MOP-130362 and PJT-173356 to J.C.T.) and the Natural Sciences and Engineering Research Council (RGPIN 03661-15 and RGPIN-2020-05174 to J.C.T.).

References

1. Allshire RC, Madhani HD. Ten principles of heterochromatin formation and function. Nat Rev Mol Cell Biol. 2018;19(4):229–44.
2. Zhu Q, Hoong N, Aslanian A, Hara T, Benner C, Heinz S, et al. Heterochromatin-Encoded Satellite RNAs Induce Breast Cancer. Mol Cell. 2018;70(5).
3. Ting DT, Lipson D, Paul S, Brannigan BW, Akhavanfard S, Coffman EJ, et al. Aberrant Overexpression of Satellite. Science. 2011;331(February):593–7.
4. Piunti A, Shilatifard A. The roles of Polycomb repressive complexes in mammalian development and cancer. Nat Rev Mol Cell Biol. 2021;22(5):326–45.
5. Tatarakis A, Behrouzi R, Moazed D. Evolving Models of Heterochromatin: From Foci to Liquid Droplets. Vol. 67, Molecular Cell. 2017.
6. Jaensch ES, Zhu J, Cochrane JC, Marr SK, Oei TA, Damle M, et al. A Polycomb domain found in committed cells impairs differentiation when introduced into PRC1 in pluripotent cells. Mol Cell. 2021;81(22):4677-4691.e8.
7. Strom AR, Emelyanov A V., Mir M, Fyodorov D V., Darzacq X, Karpen GH. Phase separation drives heterochromatin domain formation. Nat Publ Gr. 2017;547(7662):241–5.
8. Holoch D, Moazed D. RNA-mediated epigenetic regulation of gene expression. Nat Rev Genet. 2015;16(2):71–84.
9. Zhou H, Stein CB, Shafiq TA, Shipkovenska G, Kalocsay M, Paulo JA, et al. Rixosomal RNA degradation contributes to silencing of Polycomb target genes. Nature. 2022;604(7904):167–74.

10. Seczynska M, Bloor S, Cuesta SM, Lehner PJ. Genome surveillance by HUSH-mediated silencing of intronless mobile elements. Nature. 2022;601(7893):440–5.

11. Volpe TA, Kidner C, Hall IM, Teng G, Grewal SIS, Martienssen RA. Regulation of heterochromatic silencing and histone H3 lysine-9 methylation by RNAi. Science (80-). 2002;297(5588):1833–7.

12. Ira M. Hall, Gurumurthy D. Shankaranarayana, Ken-ichi Noma, Nabieh Ayoub, Amikam Cohen SISG. Establishment and Maintenance of a Heterochromatin Domain. Science (80-). 2002;297(5590):2232–7.

13. Martienssen R, Moazed D. RNAi and heterochromatin assembly. Cold Spring Harb Perspect Biol. 2015;7(8).

14. Sugiyama T, Cam H, Moazed D, Grewal SIS. RNA-dependent RNA polymerase is an essential component of a self-enforcing loop coupling heterochromatin assembly to siRNA production. 2005;102(1):1–6.

15. Colmenares SU, Buker SM, Buhler M, Dlakić M, Moazed D. Coupling of Double-Stranded RNA Synthesis and siRNA Generation in Fission Yeast RNAi. Mol Cell. 2007;27(3):449–61.

16. Noma KI, Sugiyama T, Cam H, Verdel A, Zofall M, Jia S, et al. RITS acts in cis to promote RNA interference-mediated transcriptional and post-transcriptional silencing. Nat Genet. 2004;36(11):1174–80.

17. Verdel A, Jia S, Gerber S, Sugiyama T, Gygi S, Grewal SIS, et al. RNAi-Mediated Targeting of Heterochromatin by the RITS Complex. Science (80-). 2004;

18. Motamedi MR, André V, Colmenares SU, Gerber SA, Gygi SP, Moazed D. Two RNAi Complexes, RITS and RDRC, Physically Interact and Localize to Noncoding

Centromeric RNAs Mohammad. Cell. 2004;119(5):789–802.

19. Shimada Y, Mohn F, Bühler M. The RNA-induced transcriptional silencing complex targets chromatin exclusively via interacting with nascent transcripts. Genes Dev. 2016;30(23).

20. Bayne EH, White SA, Kagansky A, Bijos DA, Sanchez-pulido L, Hoe K, et al. Stc1 : A Critical Link between RNAi and Chromatin Modification Required for Heterochromatin Integrity. Cell. 2010;140:666–77.

21. Chen ES, Zhang K, Nicolas E, Cam HP, Zofall M, Grewal SIS. Cell cycle control of centromeric repeat transcription and heterochromatin assembly. 2008;451(February):4–7.

22. Kloc A, Zaratiegui M, Nora E, Martienssen R. RNA Interference Guides Histone Modification during the S Phase of Chromosomal Replication. Curr Biol. 2008;18(7):490–5.

23. Sanulli S, Trnka MJ, Dharmarajan V, Tibble RW, Pascal BD, Burlingame AL, et al. HP1 reshapes nucleosome core to promote phase separation of heterochromatin. Nature. 2019;575(7782):390–4.

24. Al-Sady B, Madhani HD, Narlikar GJ. Division of labor between the chromodomains of HP1 and Suv39 methylase enables coordination of heterochromatin spread. Mol Cell. 2013;51:80–91.

25. Wang J, Tadeo X, Hou H, Tu PG, Thompson J, Iii JRY, et al. Epe1 recruits BET family bromodomain protein Bdf2 to establish heterochromatin boundaries. 2013;1886–902.

26. Greenstein RA, Barrales RR, Sanchez NA, Bisanz JE, Braun S, Al-Sady B.

Set1/COMPASS repels heterochromatin invasion at euchromatic sites by disrupting Suv39/Clr4 activity and nucleosome stability. Genes Dev. 2020;34(1–2):99–117.

27. Greenstein RA, Jones SK, Spivey EC, Rybarski JR, Finkelstein IJ, Al-Sady B. Noncoding RNA-nucleated heterochromatin spreading is intrinsically labile and requires accessory elements for epigenetic stability. Elife. 2018;7.
28. Dong W, Oya E, Zahedi Y, Prasad P, Svensson JP, Lennartsson A, et al. Abo1 is required for the H3K9me2 to H3K9me3 transition in heterochromatin. Sci Rep. 2020;10(1):1–13.
29. Kowalik KM, Shimada Y, Flury V, Stadler MB, Batki J, Buhler M. The Paf1 complex represses small-RNA-mediated epigenetic gene silencing ¨. Nature. 2015;520:248–52.
30. Iida T, Nakayama J ichi, Moazed D. siRNA-Mediated Heterochromatin Establishment Requires HP1 and Is Associated with Antisense Transcription. Mol Cell. 2008;31(2):178–89.
31. Shimada Y, Carl SH, Skribbe M, Flury V, Kuzdere T, Kempf G, et al. An enhancer screen identifies new suppressors of small-RNA-mediated epigenetic gene silencing. PLoS Genet. 2021;17(6):1–21.
32. Yu R, Wang X, Moazed D. Epigenetic inheritance mediated by coupling of RNAi and histone H3K9 methylation. Nature. 2018;
33. Chalamcharla VR, Folco HD, Dhakshnamoorthy J, Grewal SIS. Conserved factor Dhp1/Rat1/Xrn2 triggers premature transcription termination and nucleates heterochromatin to promote gene silencing. Proc Natl Acad Sci.

2015;112(51):15548–55.

34. Lee SY, Hung S, Esnault C, Pathak R, Johnson KR, Bankole O, et al. Dense Transposon Integration Reveals Essential Cleavage and Polyadenylation Factors Promote Heterochromatin Formation. Cell Rep. 2020;30(8):2686–98.

35. Zofall M, Yamanaka S, Reyes-Turcu FE, Zhang K, Rubin C, Grewal SIS. RNA elimination machinery targeting meiotic mRNAs promotes facultative heterochromatin formation. Science (80-). 2012;335(6064):96–100.

36. Sugiyama T, Cam HP, Sugiyama R, Noma K, Zofall M, Kobayashi R. SHREC , an Effector Complex for Heterochromatic Transcriptional Silencing. 2007;491–504.

37. Yamada T, Fischle W, Sugiyama T, Allis CD, Grewal SIS. The nucleation and maintenance of heterochromatin by a histone deacetylase in fission yeast. Mol Cell. 2005;20(2):173–85.

38. Vo T V., Dhakshnamoorthy J, Larkin M, Zofall M, Thillainadesan G, Balachandran V, et al. CPF Recruitment to Non-canonical Transcription Termination Sites Triggers Heterochromatin Assembly and Gene Silencing. Cell Rep. 2019;28:267-281.e5.

39. Reyes-Turcu FE, Grewal SIS. Different means, same end-heterochromatin formation by RNAi and RNAi-independent RNA processing factors in fission yeast. Curr Opin Genet Dev. 2012;22:156–63.

40. Reyes-Turcu FE, Zhang K, Zofall M, Chen E, Grewal SIS. Defects in RNA quality control factors reveal RNAi-independent nucleation of heterochromatin. Nat Struct Mol Biol. 2010;18(10):1132–8.

41. Reddy BD, Wang Y, Niu L, Higuchi EC, Marguerat SB, Bähler J, et al. Elimination

of a specific histone H3K14 acetyltransferase complex bypasses the RNAi pathway to regulate pericentric heterochromatin functions. Genes Dev. 2011;25(3):214–9.

42. Fitz J, Neumann T, Steininger M, Wiedemann EM, Garcia AC, Athanasiadis A, et al. Spt5-mediated enhancer transcription directly couples enhancer activation with physical promoter interaction. Nat Genet. 2020;52:505–15.

43. Aoi Y, Takahashi Y hei, Shah AP, Iwanaszko M, Rendleman EJ, Khan NH, et al. SPT5 stabilization of promoter-proximal RNA polymerase II. Mol Cell. 2021;81:4413-4424.e5.

44. Hu S, Peng L, Xu C, Wang Z, Song A, Chen FX. SPT5 stabilizes RNA polymerase II, orchestrates transcription cycles, and maintains the enhancer landscape. Mol Cell. 2021;81:4425–39.

45. Shetty A, Kallgren SP, Demel C, Maier KC, Spatt D, Alver BH, et al. Spt5 Plays Vital Roles in the Control of Sense and Antisense Transcription Elongation. Mol Cell. 2017;66:77–88.

46. Bernecky C, Plitzko JM, Cramer P. Structure of a transcribing RNA polymerase II-DSIF complex reveals a multidentate DNA-RNA clamp. Nat Struct Mol Biol. 2017;24(10):809–15.

47. Vos SM, Farnung L, Urlaub H, Cramer P. Structure of paused transcription complex Pol II–DSIF–NELF. Nature. 2018;560:601–606.

48. Hartzog GA, Fu J. The Spt4-Spt5 complex: A multi-faceted regulator of transcription elongation. Biochim Biophys Acta - Gene Regul Mech. 2013;1829:105–15.

49. Song A, Chen FX. The pleiotropic roles of SPT5 in transcription. Transcription. 2022;13(1–3):53–69.

50. Yamada T, Yamaguchi Y, Inukai N, Okamoto S, Mura T, Handa H. P-TEFb-mediated phosphorylation of hSpt5 C-terminal repeats is critical for processive transcription elongation. Mol Cell. 2006;21(2):227–37.

51. Cortazar MA, Sheridan RM, Erickson B, Fong N, Glover-Cutter K, Brannan K, et al. Control of RNA Pol II Speed by PNUTS-PP1 and Spt5 Dephosphorylation Facilitates Termination by a “Sitting Duck Torpedo” Mechanism. Mol Cell. 2019;76:896–908.

52. Parua PK, Booth GT, Sansó M, Benjamin B, Tanny JC, Lis JT, et al. A Cdk9-PP1 switch regulates the elongation-termination transition of RNA polymerase II. Nature. 2018;558(7710):460–4.

53. Page V, Lee KM, Viladevall L, Sanso M, Nagy S, Racine A, et al. A Positive Feedback Loop Links Opposing Functions of P-TEFb / Cdk9 and Histone H2B Ubiquitylation to Regulate Transcript Elongation in Fission Yeast. 2012;8(8).

54. Zhou K, Kuo WHW, Fillingham J, Greenblatt JF. Control of transcriptional elongation and cotranscriptional histone modification by the yeast BUR kinase substrate Spt5. Proc Natl Acad Sci U S A. 2009;106(17):6956–61.

55. Wier AD, Mayekar MK, Héroux A, Arndt KM, Vandemark AP. Structural basis for Spt5-mediated recruitment of the Paf1 complex to chromatin. Proc Natl Acad Sci. 2013;110(43):17290–5.

56. Mbogning J, Nagy S, Pagé V, Schwer B, Shuman S, Fisher RP, et al. The PAF Complex and Prf1 / Rtf1 Delineate Distinct Cdk9-Dependent Pathways Regulating

Transcription Elongation in Fission Yeast. PLoS Genet. 2013;9(12):e1004029.

57. Oss SB Van, Shirra MK, Bataille AR, Vandemark AP, Pugh BF, Arndt KM, et al. The Histone Modification Domain of Paf1 Complex Subunit Rtf1 Directly Stimulates H2B Ubiquitylation through an Interaction with Rad6 Article The Histone Modification Domain of Paf1 Complex Subunit Rtf1 Directly Stimulates H2B Ubiquitylation through an Int. 2016;815–25.

58. Žumer K, Maier KC, Farnung L, Jaeger MG, Rus P, Winter G, et al. Two distinct mechanisms of RNA polymerase II elongation stimulation in vivo. Mol Cell. 2021;81(15):3096-3109.e8.

59. Vos SM, Farnung L, Linden A, Urlaub H, Cramer P. Structure of complete Pol II–DSIF–PAF–SPT6 transcription complex reveals RTF1 allosteric activation. Nat Struct Mol Biol. 2020;27(7):668–77.

60. Wen Y, Shatkin AJ. Transcription elongation factor hSPT5 stimulates mRNA capping. Genes Dev. 1999;13(14):1774–9.

61. Tellier M, Maudlin I, Murphy S. Transcription and splicing: A two-way street. Wiley Interdiscip Rev RNA. 2020;11(5).

62. Doamekpor SK, Sanchez AM, Schwer B, Shuman S, Lima CD. How an mRNA capping enzyme reads distinct RNA polymerase II and Spt5 CTD phosphorylation codes. Genes Dev. 2014;28(12):1323–36.

63. Pei Y, Shuman S. Interactions between fission yeast mRNA capping enzymes and elongation factor Spt5. J Biol Chem. 2002;277(22):19639–48.

64. Kachaev ZM, Lebedeva LA, Kozlov EN, Shidlovskii Y V. Interplay of mRNA capping and transcription machineries. Biosci Rep. 2020;40(1):1–10.

65. Schneider S, Pei Y, Shuman S, Schwer B. Separable Functions of the Fission Yeast Spt5 Carboxyl-Terminal Domain (CTD) in Capping Enzyme Binding and Transcription Elongation Overlap with Those of the RNA Polymerase II CTD. Mol Cell Biol. 2010;30(10):2353–64.

66. Verrier L, Taglini F, Barrales RR, Webb S, Urano T, Braun S, et al. Global regulation of heterochromatin spreading by Leo1. Open Biol. 2015;5(150045).

67. Parsa JY, Boudoukha S, Burke J, Homer C, Madhani HD. Polymerase pausing induced by sequence-specific RNA-binding protein drives heterochromatin assembly. Genes Dev. 2018;32(13–14).

68. Chen JJ, Mbogning J, Hancock MA, Majdpour D, Madhok M, Nassour H. Spt5 Phosphorylation and the Rtf1 Plus3 Domain Promote Rtf1 Function through Distinct Mechanisms. Mol Cell Biol. 2020;40(15):e00150-20.

69. Warner MH, Roinick KL, Arndt KM. Rtf1 Is a Multifunctional Component of the Paf1 Complex That Regulates Gene Expression by Directing Cotranscriptional Histone Modification. Mol Cell Biol. 2007;27(17):6103–15.

70. Kecman T, Kuś K, Heo DH, Duckett K, Birot A, Liberatori S, et al. Elongation/Termination Factor Exchange Mediated by PP1 Phosphatase Orchestrates Transcription Termination. Cell Rep. 2018;259–69.

71. Sadeghi L, Prasad P, Ekwall K, Cohen A, Svensson JP. The Paf1 complex factors Leo1 and Paf1 promote local histone turnover to modulate chromatin states in fission yeast. EMBO Rep. 2015;16(12):1673–87.

72. Harlen KM, Churchman LS. The code and beyond: Transcription regulation by the RNA polymerase II carboxy-terminal domain. Nat Rev Mol Cell Biol.

2017;18(4):263–73.

73. Guo YE, Manteiga JC, Henninger JE, Sabari BR, Agnese AD, Shrinivas K, et al. Pol II phosphorylation regulates a switch between transcriptional and splicing condensates. Nature. 2019;572:543–8.

74. Gallego LD, Schneider M, Mittal C, Romanauska A, Gudino Carrillo RM, Schubert T, et al. Phase separation directs ubiquitination of gene-body nucleosomes. Nature. 2020;579(7800):592–7.

75. Schwer B, Schneider S, Pei Y, Aronova A, Shuman S. Characterization of the Schizosaccharomyces pombe Spt5-Spt4 complex. Rna. 2009;15(7):1241–50.

76. Moreno S, Klar A, Nurse P. Molecular genetic analysis of fission yeast Schizosaccharomyces pombe. In: Methods in Enzymology. 1991. p. 795–823.

77. Bähler J, Wu JQ, Longtine MS, Shah NG, McKenzie A, Steever AB, et al. Heterologous modules for efficient and versatile PCR-based gene targeting in Schizosaccharomyces pombe. Yeast. 1998;14(10):943–51.

78. Escorcia W, Forsburg SL. Random Spore Analysis in Fission Yeast BT - Schizosaccharomyces pombe: Methods and Protocols. In: Singleton TL, editor. New York, NY: Humana Press, New York, NY; 2018. p. 189–95. Available from: https://doi.org/10.1007/978-1-4939-7546-4_17

79. Sansó M, Parua PK, Pinto D, Peter Svensson J, Pagé V, Bitton DA, et al. Cdk9 and H2Bub1 signal to Clr6-CII/Rpd3S to suppress aberrant antisense transcription. Nucleic Acids Res. 2020;48(13):7154–68.

Figure Legends

Figure 1. *spt5-T1A* and *spt5*Δ*C* allow siRNA-mediated heterochromatin formation in *trans*. **(A)** Schematic of reporter gene system used to detect siRNA-directed *trans*-silencing. The copy of *ade6*$^+$ inserted into the heterochromatic *dg* repeats acts as an siRNA source. **(B)** Example image of *spt5(7)-T1A* colonies on adenine-limiting media. **(C)** Frequency of red colonies formed by *spt5* mutants and controls expressing *ade6*$^+$ from the *dg* locus. ~1000 cells from each genotype were plated on adenine-limiting media. Error bars indicate SEM (n=4). **(D)** Anti-H3K9me3 ChIP-qPCR using cells originating from red or white colonies as indicated; *clr4*Δ was included as a negative control. Percent input at *vtc4*$^+$ was normalized to *S. cerevisiae* spike-in. Error bars indicate SEM. Asterisks indicate significant differences for the indicated comparisons [$p<0.05$, one-way ANOVA followed by Sidak's multiple comparison test (unpaired) with a single pooled variance; n=3].

Figure 2. *spt5-T1A* and *spt5*Δ*C* allow aberrant heterochromatin spreading at *irc1*. **(A)** Schematic showing *ura4*$^+$ reporter gene construct used to detect heterochromatin spreading at *irc1*. **(B) and (C)** Spot tests of indicated *spt5* mutants on control PMG media, PMG lacking uracil, and PMG with 5'FOA. Plates were incubated at 30 degrees for 7 days before imaging.

Figure 3. A truncated Spt5 CTD allows pericentric heterochromatin formation in the absence of the RNAi pathway. **(A)** Spot tests of the indicated strains on control

media (YES) or YES containing thiabendazole (TBZ). Plates were incubated for 3 days at 30 degrees before imaging. **(B)** Anti-H3K9me3 ChIP-qPCR quantified with primers amplifying the *dh* repeat in the indicated strains. Percent input was normalized to *S. cerevisiae* spike-in. Error bars indicate SEM. Asterisks indicate significant differences for the indicated comparisons [$p<0.05$ for 1 star, $p<0.01$ for 2 stars, $p<0.001$ for 3 stars, one-way ANOVA followed by Sidak's multiple comparison test (unpaired) with a single pooled variance; n=3]. **(C)** Strand-specific RT-qPCR analysis of *dh* repeat transcripts in the indicated strains. Transcript levels measured with *dh* primers were normalized to *act1*$^{+}$ and the wild-type (WT) normalized value was set to 1 [$p<0.05$ for 1 star, $p<0.01$ for 2 stars, $p<0.001$ for 3 stars, one-way ANOVA followed by Sidak's multiple comparison test (unpaired) with a single pooled variance; n=3).

Figure 4. Blocking or mimicking phosphorylation of the Spt5 CTD T1 residue is not sufficient to rescue heterochromatin formation in the absence of the RNAi pathway. **(A)** Spot tests of the indicated strains on control media (YES) or YES containing thiabendazole (TBZ). Plates were incubated for 3 days at 30 degrees before imaging. **(B)** Anti-H3K9me3 ChIP-qPCR quantified with primers amplifying the *dh* repeat in the indicated strains. Percent input was normalized to *S. cerevisiae* spike-in. Error bars indicate SEM. Asterisks indicate significant differences for the indicated comparisons [$p<0.05$ for 1 star, $p<0.01$ for 2 stars, $p<0.001$ for 3 stars, one-way ANOVA followed by Sidak's multiple comparison test (unpaired) with a single pooled variance; n=3). **(C)** Cartoon model depicting the distinct mechanisms of heterochromatin regulation by Spt5 CTD T1 phosphorylation (top) and Spt5 CTD repeat number

(bottom).

Figure 5. Evidence that negative effects of Spt5 CTD T1 phosphorylation on heterochromatin are mediated by Prf1/Rtf1. (A) Frequency of red colonies formed by *spt5* mutants and controls expressing *ade6*$^{+}$ from the *dg* locus. ~1000 cells from each genotype were plated on adenine-limiting media. Error bars indicate SEM (n=4). **(B)** Spot tests of the indicated *prf1* mutants or controls harboring the *irc1::ura4*+ reporter gene on the indicated media. Plates were incubated at 30 degrees for 7 days before imaging. **(C)** Spot tests of the indicated strains on control media (YES) or YES containing thiabendazole (TBZ). Plates were incubated for 3 days at 30 degrees before imaging.

Figure S1. Mitotic stability of the colony color phenotypes for the indicated mutant strains harboring the dual *ade6*$^{+}$ reporter system. For each row of spots, a white or red originator colony from agar plates seeded at single cell density as in Fig. 1C was dissociated in 100 ul of water, then 5X serial dilutions were carried out for spot tests on adenine limiting media (PMG with 7mg/L adenine) and grown for 7 days at 30 degrees. An *ade6* mutant (*ade6-M210*) was included for comparison.

Figure S2. Effects of *spt5* mutants on endogenous *ura4*$^{+}$ expression and on H3K9me beyond the *irc1R* boundary element. (A) Spot tests of indicated *spt5* mutants on control PMG media and PMG lacking uracil. Plates were incubated at 30

degrees for 3 days before imaging. **(B)** Anti-H3K9me2 ChIP-qPCR in indicated *spt5* mutants and controls. Primers amplify a region outside of the *irc1R* boundary (osIRC1R). Percent input was normalized to mouse spike-in. *clr4*Δ was included as a negative control. Error bars indicate SEM (n=3). **(C and D)** As in (B) for anti-H3K9me3 ChIP-qPCR. Percent input was normalized to *S. cerevisiae* spike-in.

Figure S3. Characterization of bypass of the RNAi pathway by Spt5 CTD truncation. (A) Spot tests of the indicated strains on control media (YES) or YES containing thiabendazole (TBZ). Plates were incubated for 3 days at 30 degrees before imaging. **(B and C)** Anti-H3K9me3 ChIP-qPCR quantified with osIRC1R primers in the indicated strains. Percent input was normalized to *S. cerevisiae* spike-in. Error bars indicate SEM. Asterisks indicate significant differences between indicated comparisons [$p<0.05$ for 1 star, $p<0.01$ for 2 stars, $p<0.001$ for 3 stars, one-way ANOVA followed by Sidak's multiple comparison test (unpaired) with a single pooled variance; n=3).

Table 1. *S. pombe* strains used in this study.

Strain	Genotype	Source
JT362	*h+ leu1-32 ura4-D18 his3-D1 ade6-M210*	(56)
JT249	*h+ leu1-32 ade6-M210 ura4DS/E otr1R(SphI)::ura4 oriA clr4Δ::kanmx6*	D. Moazed
JT340	*h- spt5(7)::ura4+ leu1-32 ura4-D18 his3-D1 ade6-M210*	B. Schwer
JT341	*h- spt5(7)-T1A::ura4+ leu1-32 ura4-D18 his3-D1 ade6+*	B. Schwer
JT342	*h- spt5(7)-T1E::ura4+ leu1-32 ura4-D18 his3-D1 ade6+*	B. Schwer
JT343	*h- spt5ΔC::ura4+ leu1-32 ura4-D18 his3-D1 ade6+*	B. Schwer
JT866	*h? irc1L::ura4+ spt5ΔC::kanmx6 leu? ura4D-18 ade6?*	This study
JT871	*h? spt5ΔC::kanMx6 leu1+ ura4+ ade6?*	(56)
JT921	*h- prf1ΔC(1-345)-TAP::kanmx6 ade6-M216*	(68)
JT924	*h- prf1-R227A-TAP::kanMX6 ade6-M216*	(68)
JT926	*h- prf1-R262E-TAP::kanMX6 ade6-M216*	(68)
JT202	*h- prf1-TAP::kanMX6*	(56)

JT793	*h- IRC1L (Xho1):ura4+ per1::NatR cycR? ade6-210 leu1-32 ura4-D18*	(66)
JT943	*h- ago1Δ::hph leu1-32 ura4-UTRΔ::kanmx6 ade6-M210*	D. Moazed
JT944	*h+ otr1R(SphI)::ade6+ leu1-32 ura4-D18*	D. Moazed
JT972	*h? otr1R(SphI)::ade6+ spt5(7)::ura4+ leu? ura4D18*	This study
JT973	*h? otr1R(SphI)::ade6+ spt5(7)-T1A::ura4+ leu? ura4D18*	This study
JT974	*h? otr1R(SphI)::ade6+ spt5(7)-T1E::ura4+ leu? ura4D18*	This study
JT975	*h? otr1R(SphI)::ade6+ spt5ΔC::ura4+ leu? ura4D18*	This study
JT991	*h? ago1delta::hphMX6 spt5(7)::ura4+*	This study
JT992	*h? ago1delta::hph spt5(7)-T1A::ura4+*	This study
JT993	*h? ago1delta::hph spt5(7)-T1E::ura4+*	This study
JT994	*h? ago1delta::hph spt5ΔC::ura4+*	This study
JT1030	*h- irc1L(Xho1):ura4+ per1:hph*	This study
JT1034	*h? irc1L(Xho1):ura4+ per1:hph spt5(7)::natmx6*	This study
JT1035	*h? irc1L(Xho1):ura4+ per1:hph spt5(7)-T1A::natmx6*	This study
JT1036	*h? irc1L(Xho1):ura4+ per1:hph spt5(7)-T1E::natmx6*	This study

JT1047	*h- spt5(18)::ura4+ leu1-32 ura4-D18 his3-D1 ade6-M210*	B. Schwer
JT1048	*h- spt5(18)-T1A::ura4+ leu1-32 ura4-D18 his3-D1 ade6-M210*	B. Schwer
JT1049	*h- spt5(18)-T1E::ura4+ leu1-32 ura4-D18 his3-D1 ade6-M210*	B. Schwer
JT1071	*h? spt5(7)::natmx6 leu1-32 ura4-D18 his3-D1 ade6-M210*	This study
JT1072	*h? spt5(7)-T1A::natmx6 leu1-32 ura4-D18 his3-D1 ade6-M210*	This study
JT1073	*h? spt5(7)-T1E::natmx6 leu1-32 ura4-D18 his3-D1 ade6-M210*	This study
JT1075	*h? otr1R(SphI)::ade6+ prf1-TAP::kanmx6*	This study
JT1076	*h? otr1R(SphI)::ade6+ prf1R227A-TAP::kanmx6*	This study
JT1077	*h? irc1L(Xho1)::ura4+ per1::hphMX6 prf1-TAP::kanMX6 ura4-D18*	This study
JT1104	*h? irc1L(Xho1):ura4+ per1::hphMX6 prf1R227A-TAP::kanMX6 ura4-D18*	This study
JT1105	*h? irc1L(Xho1):ura4+ per1::hphMX6 prf1ΔC(1-345)-TAP::kanMX6 ura4-D18*	This study
JT1131	*h? otr1R(SphI)::ade6+ spt5(18)::ura4+*	This study
JT1132	*h? otr1R(SphI)::ade6+ spt5(18)-T1A::ura4+*	This study
JT1133	*h? otr1R(SphI)::ade6+ spt5(18)-T1E::ura4+*	This study

JT1141	*h? otr1R(SphI)::ade6+ prf1R296E::kanmx6*	This study
JT1142	*h? otr1R(SphI)::ade6+ prf1R262E::kanmx6*	This study
JT1171	*h? ago1Δ::hph spt5(18)::ura4+*	This study
JT1172	*h? ago1Δ::hph spt5(18)-T1A::ura4+*	This study
JT1192	*h+ spt5(18)::natMX6 leu1-32 ura4-D18 his3-D1 ade6-M210*	This study
JT1193	*h+ spt5(18)-T1A::natMX6 leu1-32 ura4-D18 his3-D1 ade6-M210*	This study
JT1194	*h+ spt5(18)-T1E::natMX6 leu1-32 ura4-D18 his3-D1 ade6-M210*	This study
JT1247	*h? ago1Δ::hphMX6 spt5(18)-T1E::ura4+*	This study
JT1174	*h? dcr1Δ::hphMX6 spt5(7)::ura4+*	This study
JT1178	*h? dcr1Δ::hphMX6 spt5(7)-T1A::ura4+*	This study
JT1179	*h? dcr1Δ::hphMX6 spt5(7)-T1E::ura4+*	This study
JT1180	*h? dcr1Δ::hphMX6 spt5ΔC::ura4+*	This study
JT1248	*h? irc1L(Xho1):ura4+ per1::hphMX6 prf1R296E-TAP::kanMX6 ura4-D18*	This study
JT1245	*h? irc1L(Xho1):ura4+ per1::hphMX6 prf1R262E-TAP::kanMX6 ura4-D18*	This study
JT1308	*h? ago1Δ::hphMX6 prf1R262E-TAP*	This study
JT1309	*h? ago1Δ::hphMX6 prf1ΔC(1-345)-TAP::kanMX6*	This study
JT1310	*h? ago1Δ::hphMX6 prf1-TAP::kanmx6*	This study
JT1315	*h? ago1Δ::hphMX6 prf1R227A-TAP::kanmx6*	This study

JT1200	*h- irc1L(Xho1):ura4+ per1::hphMX6 spt5(18)::ura4+*	This study
JT1201	*h- irc1L(Xho1):ura4+ per1::hphMX6 spt5(18)-T1A::ura4+*	This study

Table 2. Oligonucleotide primers used in this study.

Primer	Sequence
Vtc4'Fw	AGCCAAACATAATGCGGTCC
Vtc4'Rv	AACATTGGCGCTGATTGCAG
Dh'Fw	ACAATTGTGACTTTGTTGGT
Dh'Rv	TGTCCATACCCATGCTGTGTC
Outside-IRC1R'Fw	GAGAGGTTTCTTATCGTGCTATC
Outside-IRC1R'Rv	GAGTGTAAACTTAGTGTGAGC
Pma1'Fw	ACCCCAGCTAGTTAAAGAAAATCA
Pma1'Rv	CGTCATCGTCAGAAGATTCAGATG
Pou5F'Fw	GTGGGTAAGCAAGAACTGAGGA
Pou5F'Rv	TGGAGAGCCTAAAACATCCATT
Ade6'Fw	GCAGGCCAAGAGTTTGGTTAT
Ade6'Rv	CCAAGTGCTTTGATGGCAGTA
Act1'Fw	CCACTATGTATCCCGGTATTGC
Act1'Rv	CAATCTTGACCTTCATGGAGCT
Dg'Fw	ACAATTAGGGCATGTGGTGT
Markerswitch'Fw	CGGATCCCCGGGTTAATTAAGGCG
Markerswitch'Rv	GAATTCGAGCTCATTTAAACACTGGATG
Spt5Ura4'Fw	GTGGGCTGCTCCCACACCAGGTG GTTGGGATGATGAAGAAGGAGAT TCACCCAAATATGTACCTCCTTCT CCTTAATAAGCGGATCCCCGGGTTAATTAA

Spt5Ura4'Rv	ACAAGATTACGTTAATTAGAATAT GTCTTAACAATTTTAACAAAACTAT CTGTCGATATTTTCAAAAATTTGAT TTTAAAGAATTCGAGCTCGTTTAAAC

Figure 1

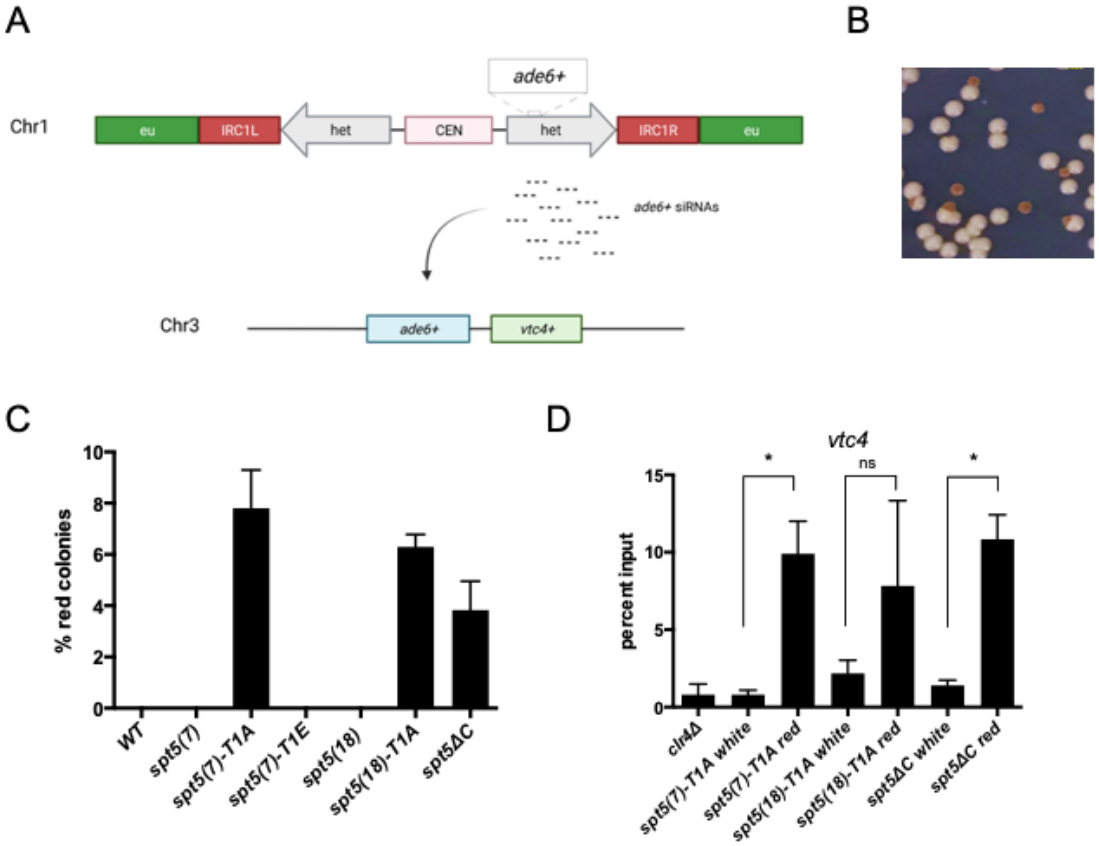
A
B
ade6+
Chr1
eu
IRC1L
het
CEN
het
IRC1R
eu
ade6+ siRNAs
Chr3
ade6+
vtc4+
C
% red colonies
10
8
6
4
2
0
WT
spt5(7)
spt5(7)-T1A
spt5(7)-T1E
spt5(18)
spt5(18)-T1A
spt5ΔC
D
vtc4
percent input
15
10
5
0
*
ns
*
clr4Δ
spt5(7)-T1A white
spt5(7)-T1A red
spt5(18)-T1A white
spt5(18)-T1A red
spt5ΔC white
spt5ΔC red

Figure 2

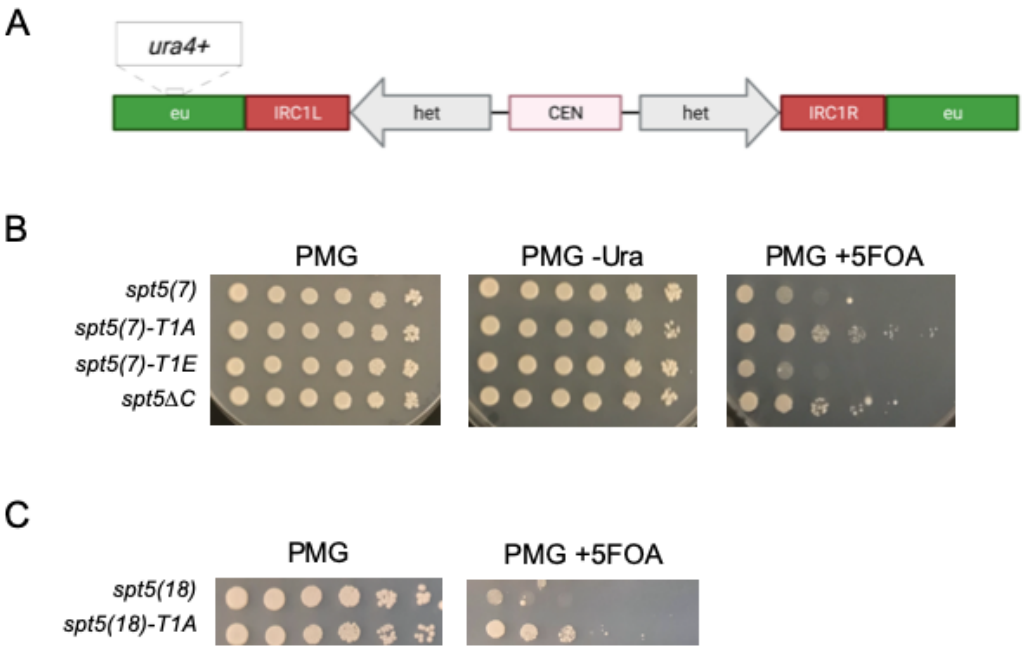
A
ura4+
eu
IRC1L
het
CEN
het
IRC1R
eu
B
PMG
PMG -Ura
PMG +5FOA
spt5(7)
spt5(7)-T1A
spt5(7)-T1E
spt5ΔC
C
PMG
PMG +5FOA
spt5(18)
spt5(18)-T1A

Figure 3

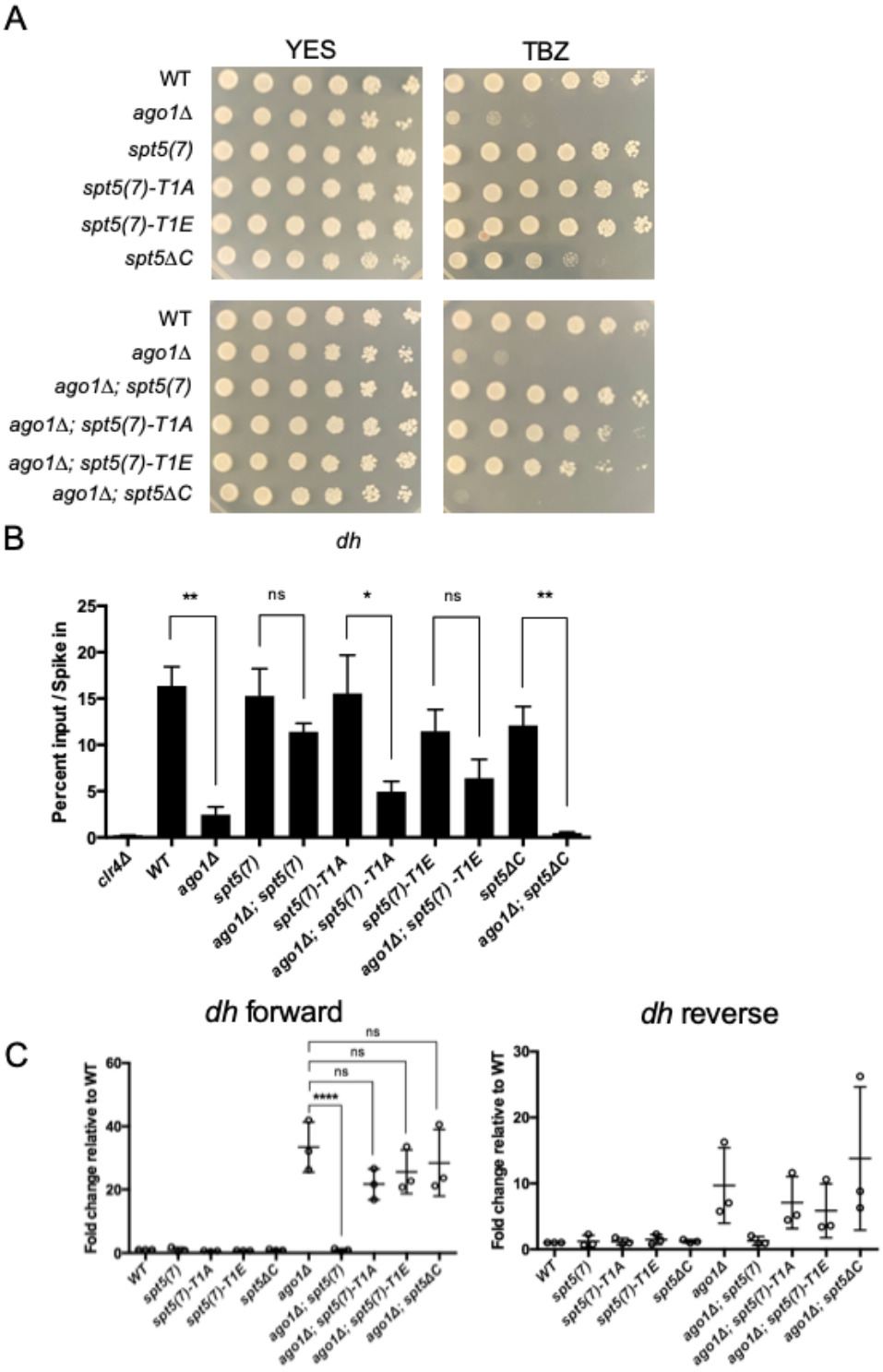
A
YES
TBZ
WT
ago1Δ
spt5(7)
spt5(7)-T1A
spt5(7)-T1E
spt5ΔC
WT
ago1Δ
ago1Δ; spt5(7)
ago1Δ; spt5(7)-T1A
ago1Δ; spt5(7)-T1E
ago1Δ; spt5ΔC
B
dh
Percent input / Spike in
clr4Δ
WT
ago1Δ
spt5(7)
ago1Δ; spt5(7)
spt5(7)-T1A
ago1Δ; spt5(7) -T1A
spt5(7)-T1E
ago1Δ; spt5(7) -T1E
spt5ΔC
ago1Δ; spt5ΔC
C
dh forward
dh reverse
Fold change relative to WT

Figure 4

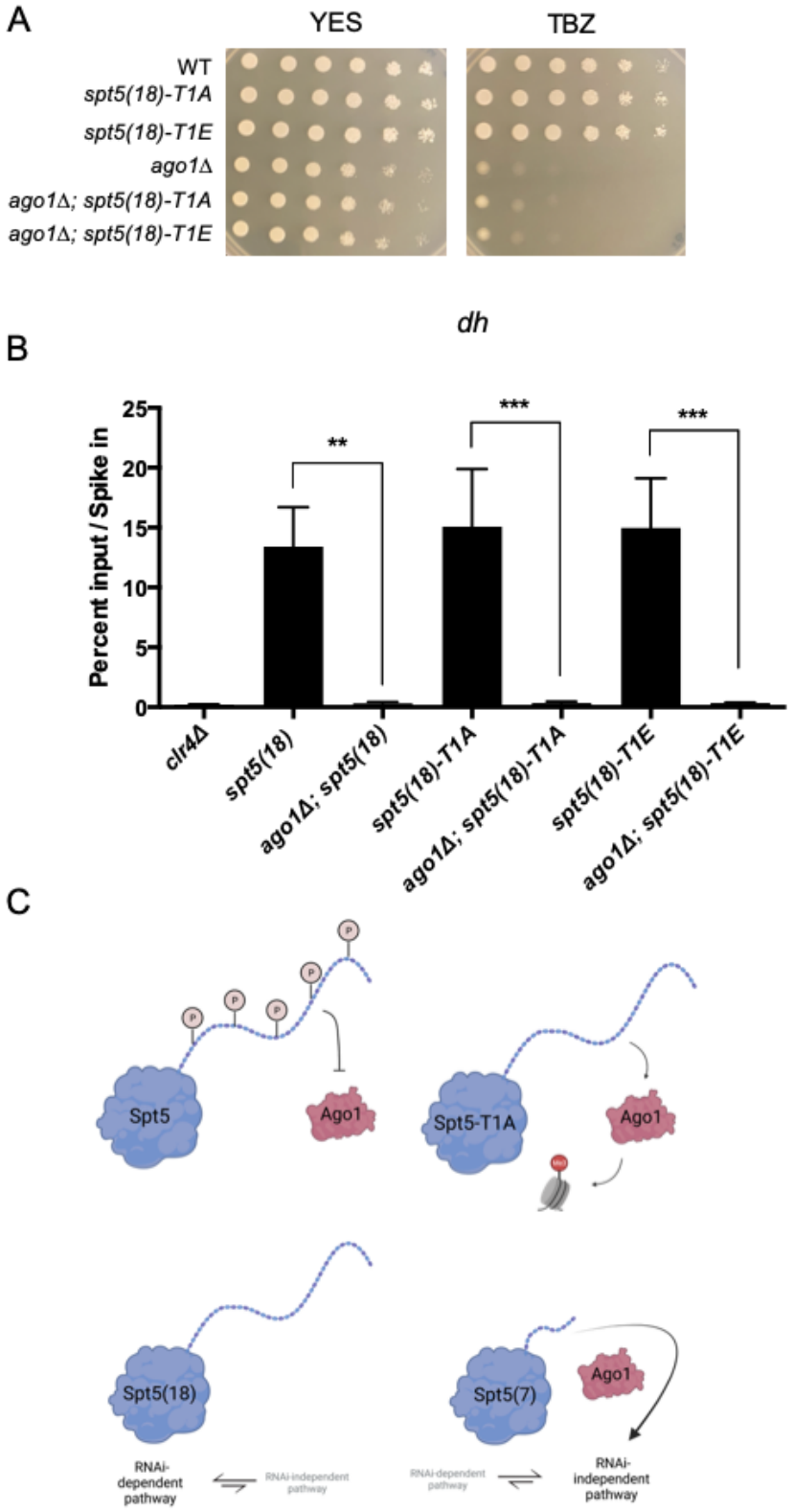
A
YES
TBZ
WT
spt5(18)-T1A
spt5(18)-T1E
ago1Δ
ago1Δ; spt5(18)-T1A
ago1Δ; spt5(18)-T1E
B
dh
Percent input / Spike in
25
20
15
10
5
0
**
***
***
clr4Δ
spt5(18)
ago1Δ; spt5(18)
spt5(18)-T1A
ago1Δ; spt5(18)-T1A
spt5(18)-T1E
ago1Δ; spt5(18)-T1E
C
Spt5
Ago1
Spt5-T1A
Ago1
Spt5(18)
Spt5(7)
Ago1
RNAi-dependent pathway
RNAi-independent pathway
RNAi-dependent pathway
RNAi-independent pathway

Figure 5

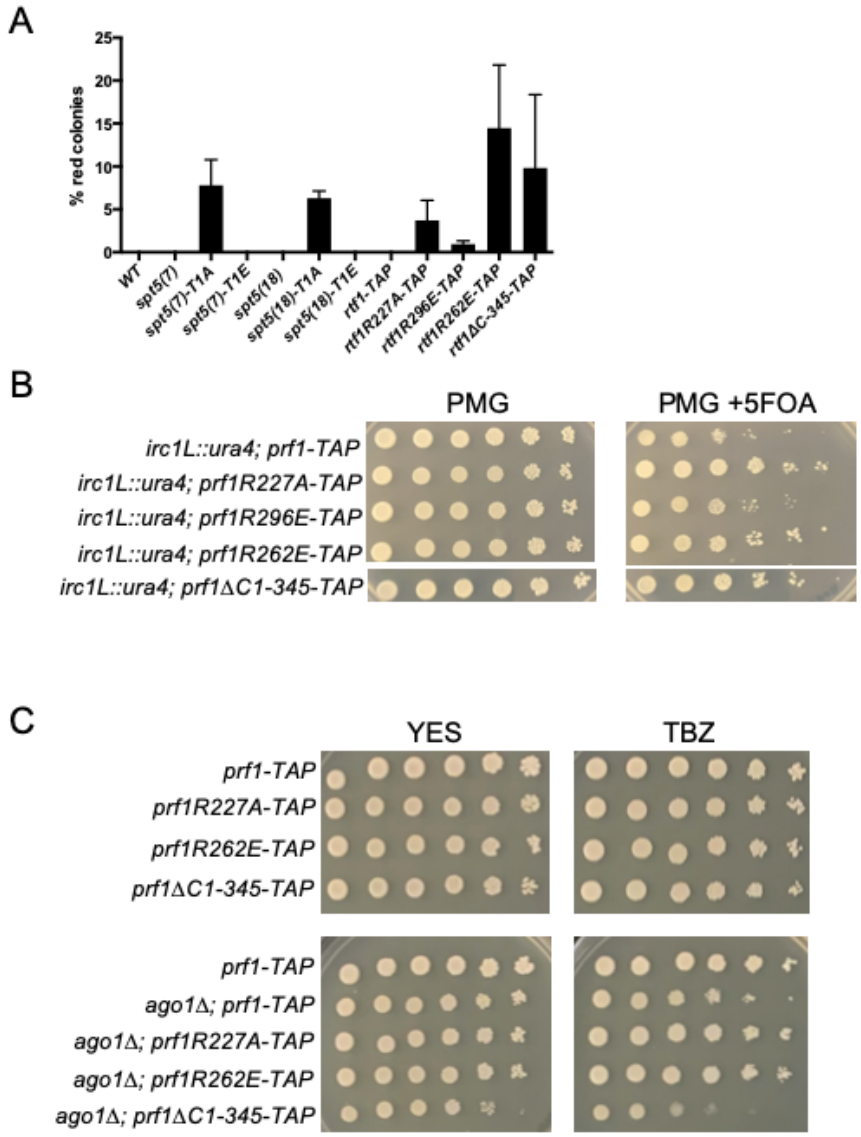
A
% red colonies
25
20
15
10
5
0
WT
spt5(7)
spt5(7)-T1A
spt5(7)-T1E
spt5(18)
spt5(18)-T1A
spt5(18)-T1E
rtf1-TAP
rtf1R227A-TAP
rtf1R296E-TAP
rtf1R262E-TAP
rtf1ΔC-345-TAP
B
PMG
PMG +5FOA
irc1L::ura4; prf1-TAP
irc1L::ura4; prf1R227A-TAP
irc1L::ura4; prf1R296E-TAP
irc1L::ura4; prf1R262E-TAP
irc1L::ura4; prf1ΔC1-345-TAP
C
YES
TBZ
prf1-TAP
prf1R227A-TAP
prf1R262E-TAP
prf1ΔC1-345-TAP
prf1-TAP
ago1Δ; prf1-TAP
ago1Δ; prf1R227A-TAP
ago1Δ; prf1R262E-TAP
ago1Δ; prf1ΔC1-345-TAP

Figure S1

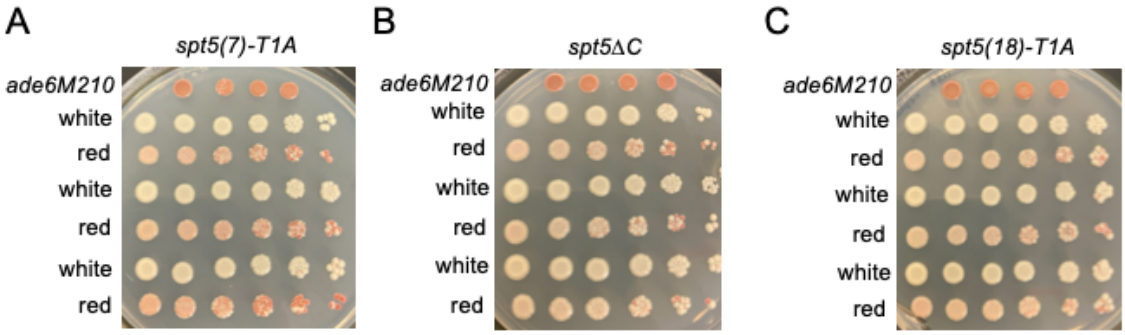

Figure S1. Mitotic assays of indicated strains harboring *ade6+* reporter system. For each row of spots, a white or red originator colony from agar plates seeded at single cell density as in Fig. 1C was dissociated in 100 ul of water, then 5X serial dilutions were carried out for spot tests on adenine limiting media (PMG with 7mg/L adenine) and grown for 7 days at 30 degrees. An ade6+ null strain (*ade6M210*) was included for comparison.

Figure S2

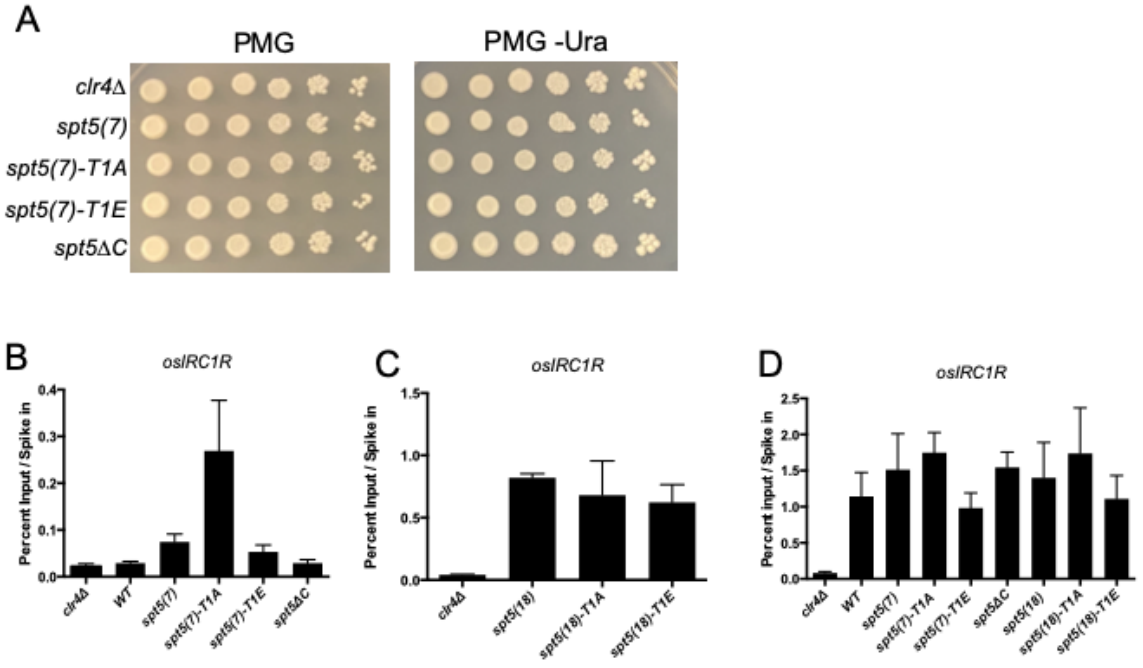
A
PMG
PMG -Ura
clr4Δ
spt5(7)
spt5(7)-T1A
spt5(7)-T1E
spt5ΔC
B
oslRC1R
Percent Input / Spike in
0.0
0.1
0.2
0.3
0.4
clr4Δ
WT
spt5(7)
spt5(7)-T1A
spt5(7)-T1E
spt5ΔC
C
oslRC1R
Percent Input / Spike in
0.0
0.5
1.0
1.5
clr4Δ
spt5(18)
spt5(18)-T1A
spt5(18)-T1E
D
oslRC1R
Percent input / Spike in
0.0
0.5
1.0
1.5
2.0
2.5
clr4Δ
WT
spt5(7)
spt5(7)-T1A
spt5(7)-T1E
spt5ΔC
spt5(18)
spt5(18)-T1A
spt5(18)-T1E

Figure S3

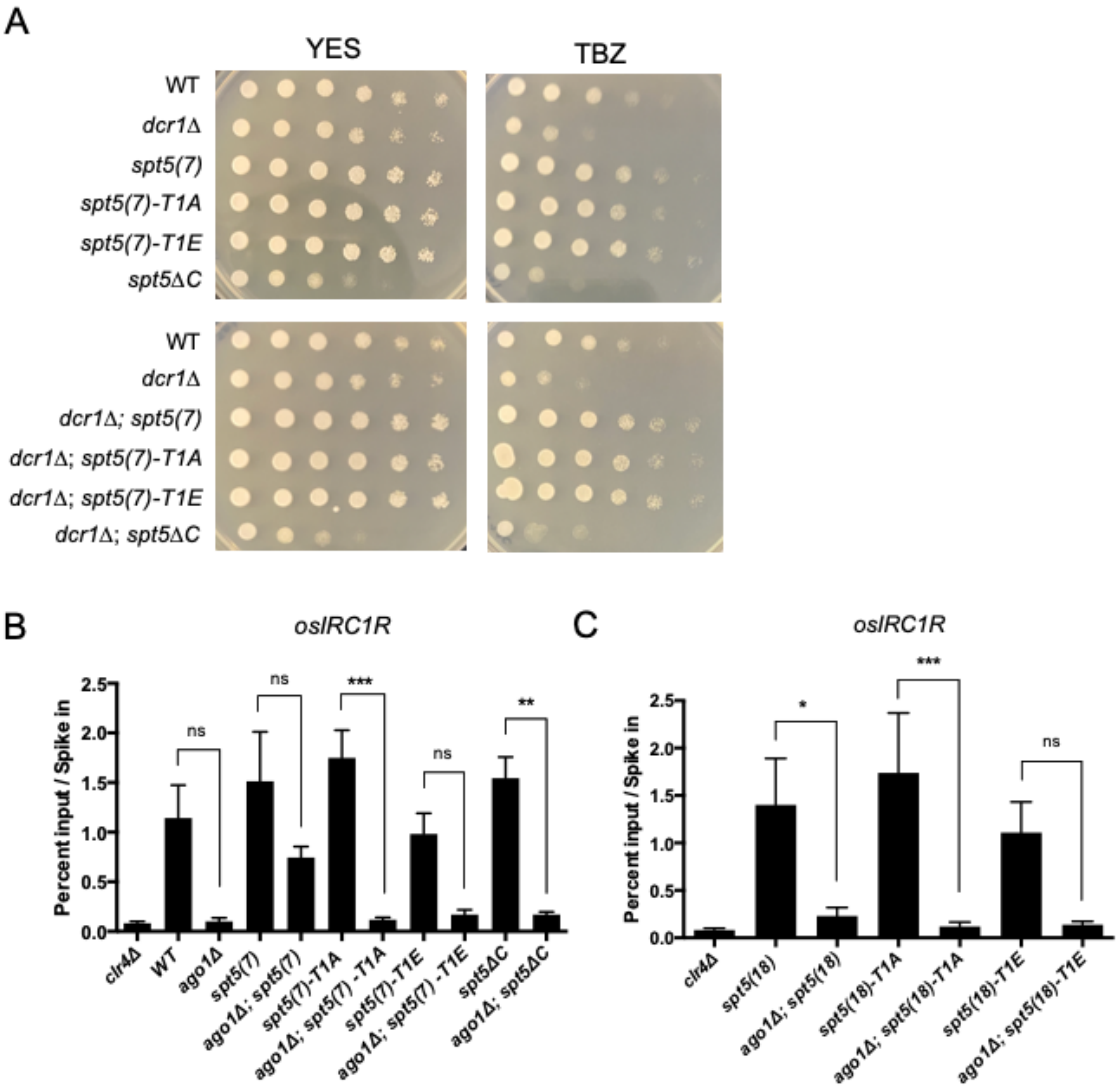
A
YES
TBZ
WT
dcr1Δ
spt5(7)
spt5(7)-T1A
spt5(7)-T1E
spt5ΔC
WT
dcr1Δ
dcr1Δ; spt5(7)
dcr1Δ; spt5(7)-T1A
dcr1Δ; spt5(7)-T1E
dcr1Δ; spt5ΔC
B
oslRC1R
Percent input / Spike in
2.5
2.0
1.5
1.0
0.5
0.0
ns
ns
***
ns
**
clr4Δ
WT
ago1Δ
spt5(7)
ago1Δ; spt5(7)
spt5(7)-T1A
ago1Δ; spt5(7) -T1A
spt5(7)-T1E
ago1Δ; spt5(7) -T1E
spt5ΔC
ago1Δ; spt5ΔC
C
oslRC1R
Percent input / Spike in
2.5
2.0
1.5
1.0
0.5
0.0
*
***
ns
clr4Δ
spt5(18)
ago1Δ; spt5(18)
spt5(18)-T1A
ago1Δ; spt5(18)-T1A
spt5(18)-T1E
ago1Δ; spt5(18)-T1E